Dispersion Relations in Plate Structures Studied with a Scanning Laser Vibrometer

Bernd KÖHLER, Fraunhofer Institute for Non-Destructive Testing, Dresden, Germany

Abstract. Scanning laser vibrometric (SLV) measurements offer a powerful tool to record and visualize the wave propagation in plates with isotropic and anisotropic properties. Snapshots and B-scans provide a good qualitative overview of the dispersion, but also numerical relations can be derived from SLV measurements, as it is demonstrated. A technique described in literature in the context of fluid coupled and air borne ultrasound is applied for laser detection of wave fields. While for isotropic plates a good quantitative agreement between experimentally determined dispersion curves and the well known Lamb wave numerical solutions can be obtained, it needs further work for anisotropic plates, to be published in a forthcoming paper.

1. Introduction

Structural Health Monitoring (SHM) aims at a permanent monitoring of structures like the airplane's outer skin or the blades of wind turbines. Therefore, the sensors reside in the structure during its whole life. Because large structures have to be monitored with a limited number of sensors, sophisticated sensor concepts and a thorough understanding of wave propagation in plates are needed. To clarify wave propagation, time resolved scanning laser vibrometric (SLV) measurements have proven efficient [1], [2].
The wave propagation in plates is characterized by various wave modes exhibiting strong geometrical dispersion. It has been shown that this dispersion can be visualized clearly using SLV. But for several advanced sensor concepts a quantitative knowledge of the dispersion is needed.

Lamb wave dispersion has been studied extensively for the determination of elastic properties. Mostly the far field of transducers in immersion technique has been exploited in these studies. Fei and Chimenti [3] introduced strongly focused water-coupled transducers to obtain high wave-number content in a single scan. In a further paper by Holland [4] focused air-coupled transducers were used, avoiding disturbance of the Lamb waves by the fluid load. In the present paper interferometric point detection is applied, which has in the spatial spectrum no limitation at all and is load free. Additionally, it is applicable to curved surfaces, allowing measurements on constructional parts e. g. the skin of airplanes, in principle. The last point is advantageous in any case where it is difficult to obtain plane plates of an identical material used in a special application. The method presented uses 2D scans of the wave field as a starting point. While already 1D line scans carry sufficient information to generate the dispersion relation, 2D scans are favorable for several reasons. First, to visualize the wave field provides an impression of the modes involved. Especially waves reflected at boundaries of the part under consideration can be identified easily and the evaluated regions can be chosen accordingly. Second, the dispersion relation is determined along lines that can be selected in directions in which the Lamb wave approximates a plane wave well.

After some theory in chapter 2 the experimental arrangement is described in chapter 3. Some visualization results in chapter 4 illustrate how the dispersion appears in 2D snapshots and in B-scans of the wave motion. Chapter 5 describes the approach how dispersion maps are generated by SLV measurements and their verification for isotropic materials. In chapter 6 this approach is applied to an anisotropic plate of a triax CFRP (Carbon Fiber Reinforced Plastics) material. Finally conclusions for further work are derived.

2. Some Theory

Fiber Reinforced Plastic (FRP) materials consist usually of several plys with varying orientation. We assume the number of plys across the plate thickness reasonably large so that average properties across the plys can be used. This approximation will be valid for wavelengths much larger than the ply thickness and certainly valid for wavelengths larger than the plate. In this approximation the plate is homogeneous but not isotropic, in general.

The elastic wave propagation in anisotropic materials is studied in a number of textbooks (see e. g. Auld [5]) where such concepts as phase and group velocity are introduced. The magnitude of the group velocity differs in general from the magnitude of the phase velocity as the direction of energy flow (equal to the direction of the group velocity vector) does from the wavefront normal ($\vec{n}$) unit vector. But for non-dissipative and linear systems the phase velocity of bulk waves is still independent of the frequency. On the other hand, the boundary condition of isotropic plates leads to the existence of dispersive wave modes even in lossless linear materials [6], [7]. Then the group velocity differs from the phase velocity but still has the direction of the k-vector ($\vec{k} = \vec{n}k$). In anisotropic plates both phenomena accrue, i. e. the phase velocity of plate waves will be frequency dependent and the corresponding group velocity vector will not be parallel to the wave front normal vector. There is some work known in literature about the calculation of wave propagation in anisotropic plates [7]-[10]. Instead of repeating the theory of elastic wave motion in homogeneous but in general anisotropic plates, only the points relevant for the subsequent considerations will be mentioned.

Without loss of generality the coordinates are chosen so that the plate is in parallel to the x-y plane. Solutions of the wave equation are supposed as superposition of plane waves. The z component of the displacement field (the measured quantity) is denoted by u_z and the position vector by $\vec{r} = x\vec{e}_x + y\vec{e}_y$. Then the plane wave solution of the wave equation can be written for u_z as

$$u_z(\vec{r},t) = u_{z0}\int d\omega\left[f(\omega)e^{i(k\vec{n}\vec{r}-\omega t)}\right] \tag{1}$$

In (1) the magnitude k of the wave vector $\vec{k} = \vec{n}k$ is in general a function of the frequency ω and of the orientation of the unit vector $\vec{n}$. Taking the double Fourier transformation of u_z with respect to its two independent variables $\vec{n}\vec{r}$ and t and denoting the transformed variables by ϑ and ω respectively, it results:

$$\tilde{\tilde{u}}(\vartheta,\omega) = F_t\left[F_{\vec{r}\vec{n}}\left[u_z(\vec{n}\vec{r},t)\right]\right] = u_{z0}\,f(\omega)\delta(\vartheta - k(\omega)) \tag{2}$$

Here F_x denotes the Fourier transformation of the function in the bracket with respect to its variable x and δ is the Dirac delta function. The phase velocity is defined as

$$v_{ph}(\omega) = \frac{\omega}{k(\omega)} \tag{3}$$

Equations (2), (3) are the basis for the determination of the phase velocity according to the following rules:

- measure a nonzero component of the wave field in a plane of the plate, this can be the out of plane component of the surface, but the derivation remains valid when other components are used,
- select areas where the wave field can be considered as consisting of plane waves to a good approximation,
- select a line normal to the wave fronts (that is a line in parallel to the vector $\vec{k}$ of the plane waves considered),
- perform a double Fourier transformation of the wave field data over the spatial coordinate along this line and over the time t,
- identify the trace of the transformed function in the (η, ω) plane, and
- calculate $v_{ph}(\omega)$ according to (3).

From the above procedure, the dispersion relation for one mode results for frequencies contained in the signal for all ω where $f(\omega)$ is significantly different from zero. Because all operations in (2) applied on the signal u_z are linear, more than one traces will appear if the wave motion can be described as superposition of several modes. But the phase velocity will be correct only for those modes having wave fronts normal to the selected transformation line.

3. Experimental Details

Several plates have been considered for demonstration. These are

a) an isotropic aluminum plate of thickness d = 1.5 mm,
b) an isotropic plate of Perspex with a thickness d = 3 mm, and
c) an anisotropic plate of glass fiber reinforced plastic (GFRP) material.

For the anisotropic material (c) the plys include 0 and +- 45 degree, while a 90 degree ply is not present. The plate thickness is 4 mm. All plates have localized inhomogeneities, representing flaws. The aluminum plate has a flat bottom hole and the GFRP plate an inserted layer. But the areas of the wave fields to be evaluated are selected as to be not much influenced by the flaws.

The transducer for excitation of plate waves were in both cases piezoelectric Lead [Plumbum] Zirconate Titanate (PZT) discs glued onto the plate surface. The disc diameter was 8 mm and the disc thickness 0.25 mm. Due to lack of disc backing the thickness resonance of the disc does not couple to the plate effectively. Instead radial displacements and radial stresses are coupled to the plate, exciting both symmetric and antisymmetric wave modes.

The voltage for exciting the PZT discs was produced in an arbitrary waveform generator and amplified by a wideband laboratory amplifier able to drive capacitive load with a voltage up to 40 V. This way both, narrow band sinusoidal and wide band pulse excitation was possible.

For detection of the waves a commercial laser vibrometer (Polytec SLV 3000) was used. The frequency bandwidth of the displacement decoder is 20 MHz. The instrument provides a voltage proportional to the particle displacement (or displacement velocity), which is digitized by a digital scope (DSO). The beam is scanned by mirrors over the sur-

face using a rectangular grid. At each grid point a measurement is undertaken and the data are transferred via IEEE interface to the computer (PC). The PC also controls the mirrors of the SLV. Evaluation programs allow displaying the data in various ways.

The amount of light collected by the interferometer determines the signal to noise ratio essentially. For enhancement of light backscattering, a retro-reflex foil was applied to the plate surface. It has been proven before that the used foil does not influence the measured displacements when the frequency is kept below 500 kHz as valid in all experiments presented.

The laser vibrometer was positioned in front of the measurement surface. So, mainly the out-of-plane vibration component was detected. Disadvantageously, the symmetric wave modes have only a small out-of-plane component and are imaged weakly. But nevertheless, as a rule they can be visualized, hence conclusions about their dispersion and directivity can be drawn.

4. Some Visualization Results

In this section some examples of wave fields detected under different conditions will illustrate how dispersion is represented in the scanned fields, as a summary of some publications. Figure 1 shows the arrangement for the experiment with an isotropic aluminum plate of 1.5 mm thickness. The area scanned by the vibrometer is indicated by a dark gray rectangle. The transducer is 20 mm distant from the detection area, so the wave fronts are moderately bended, only. The transducer was excited by a sinusoidal burst of 5 cycles with a frequency of 500 kHz.

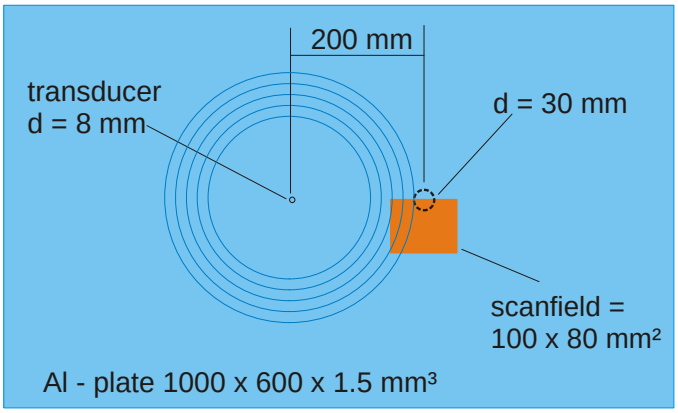

Figure 1. Experimental arrangement for generation and laser detection of Lamb waves in an aluminum plate.

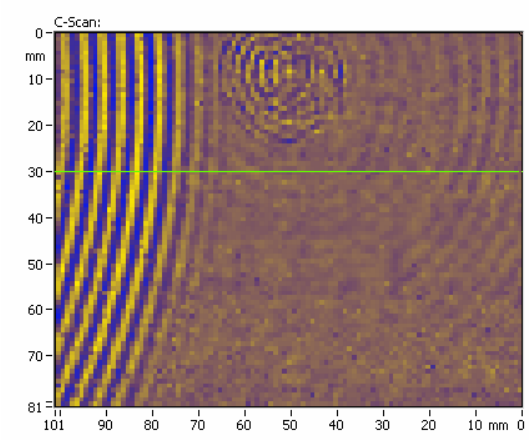

Figure 2. C-scan (snapshot of the wave field) at t = 30 µs, the horizontal and the vertical axis are given in mm.

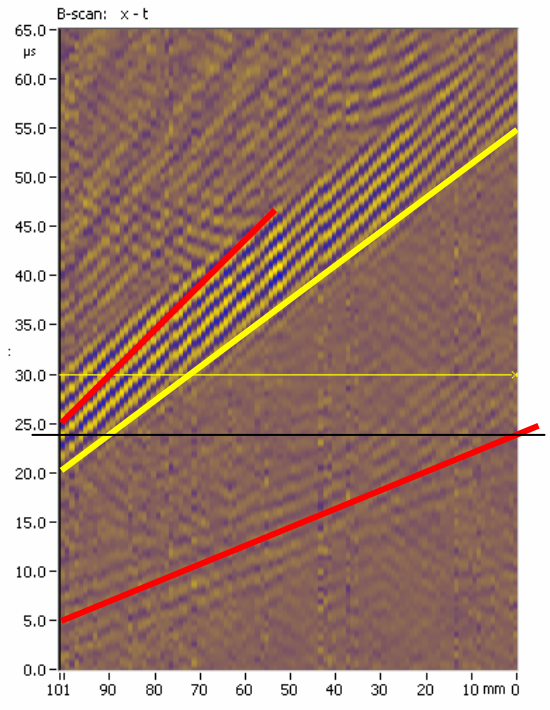

Figure 3. B-scan along the horizontal (green) line of Figure 2 (y = 30 mm).

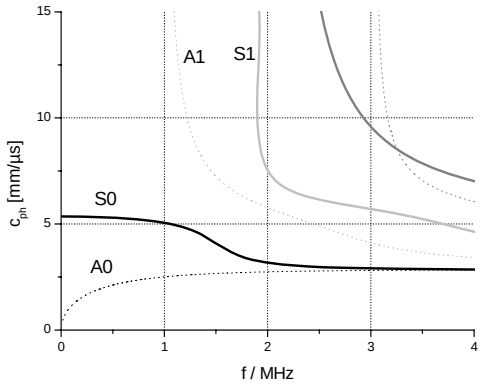

Figure 4. Phase velocity dispersion diagram for an aluminum plate of thickness d = 1.5 mm (see [11]).

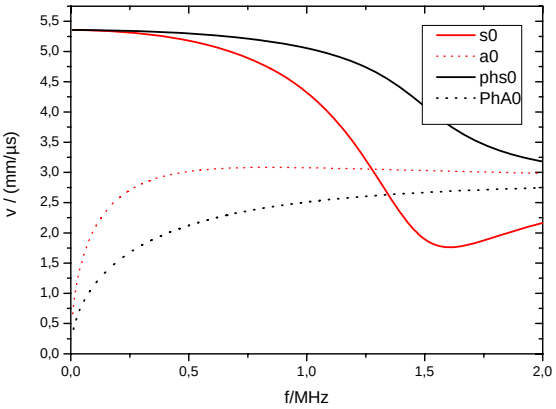

Figure 5. Group velocity (red) and phase velocity (black) for the two lowest modes of the dispersion diagram (see [11]).

Figure 2 gives a snapshot of the wave motion at t = 30 µs. An incoming wave and the defect area are clearly visible. A good insight into the wave motion can be obtained when B-scan like images are generated from the data set. This means that the displacements are plotted in an ξ-t- field while the data are taken along a properly selected line with co-ordinate ξ in the x-y scan area. Figure 3 gives a B-scan for the line parallel to the x-axis with y = 26 mm. Besides some scattered signals (due to the flat bottom hole) two main traces with a different slope are visible in this scan. The phase velocity can be determined by evaluating the slope of points of an equal phase in these traces. So the trace with the low slope belongs to the faster wave and the other to a slower one. For the fast wave obviously the slope of the phase coincides with the slope of the whole wave packet. But for the slower wave the whole packet, i. e. the envelope of the vibration, moves considerably faster than the individual waves. So, at the front of the packet new cycles are generated continuously.

The velocity of the energy of a wave packet, i. e. the velocity of its envelope, is denoted as group velocity. The two modes can be identified as S0 and A0 Lamb wave mode by comparison of the phase and group velocities with numerically determined dispersion diagrams. The values given by numerical evaluation at 500 kHz are 5.298 mm/µs and 2.123 µs/mm for the S0 and A0 mode, respectively ([11]). This is in good agreement with the values determined out of Figure 3 which are c_{Ph} = 5.26 mm/µs and c_{Ph} = 2.0 mm/µs. In case of A0 the group velocity differs from the phase velocity significantly (see Fig. 5). In good agreement are c_{gr} = 2.8 µs/mm from the measurement and the simulation value of 3.015 µs/mm. For this frequency the group velocity is approximately at a factor of 1.5 higher than the phase velocity.

In Figure 6 snapshots and B-scans are compared for excitation with different bandwidth (razed cosine with one and three cycles = RC 1 and RC 3, respectively). In the snapshots the dispersion is visible only for the high bandwidth RC1 excitation because the short wavelength signals traveled a longer distance than long wavelength parts. In the B-scan the dispersion of the A0 mode is recognizable for both the RC1 and RC3 excitation. In the wideband case a pronounced bending of the traces (points of equal phase) is apparent.

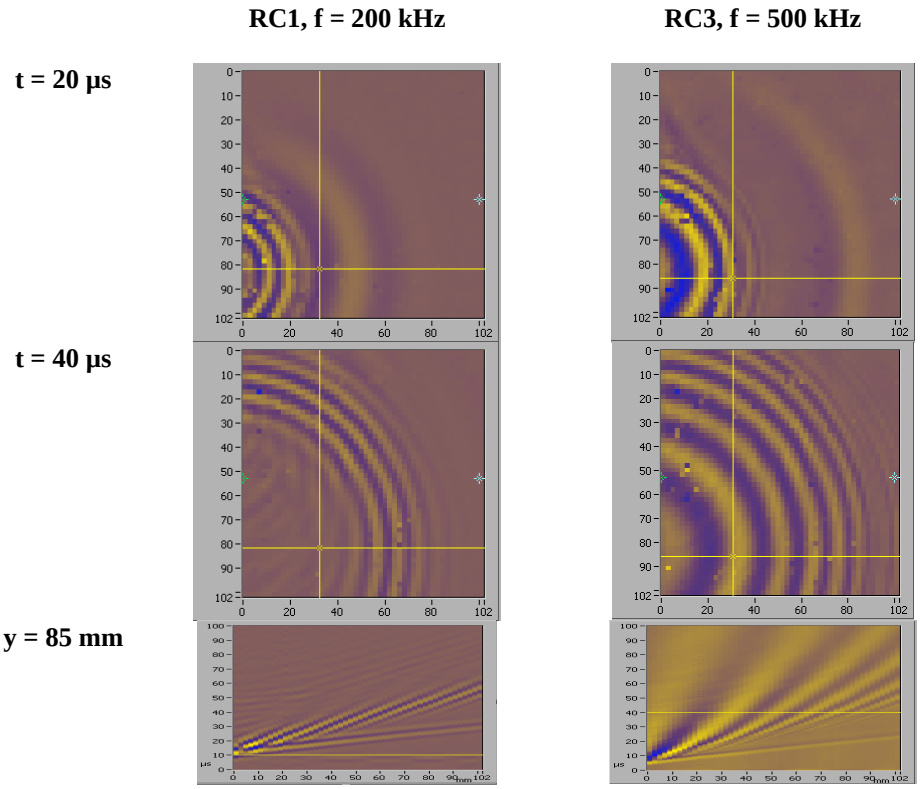

Figure 6. Snapshots and B-scans for different excitation conditions. Left: RC3 with f = 200 kHz, right: RC 1 with f = 500 kHz; upper line: snapshot at t = 20 µs, middle line: snapshot at t = 40 µs, bottom line: B-scan for a horizontal line trough the excitation point (see horizontal line in the snapshots).

5. Determination of the Dispersion Relation; Verification of the Method in the Case of Isotropic Plates

For determining the dispersion, software has been written using LabVIEW (National Instruments), allowing all necessary data handling. Figure 7 exemplifies the user interface. In the upper right window a snapshot of the wave motion is displayed. The time of the snapshot can be selected by a slider. By cursors (displayed red and yellow) the start and end point of the line used for determining the dispersion relation can be selected. The upper left two windows show the time signals at the selected points. In the lower right corner a B-scan over a horizontal line containing the yellow cursor is displayed. In the present measurement the B-scan includes the source point. The B-scan traces shown are typical for wide band excited dispersive signals. Finally, the lower left corner displays the dispersion map in the form “frequency over inverse wave length”, which is obtained by Fourier transformation of the data between the two cursors in the time and frequency domain. The operator has the option to perform several operations on the data to improve the evaluation. He may:

a) average the data over a given range in samples perpendicular to the line selected for evaluation, and
b) set various windows in the time domain.

The option (a) is useful when the signal is noisy: averaging over the neighbor lines reduces the noise. Very often the structure is not large enough to avoid reflections from structure edges. In the B-scan of Figure 7 such reflections are visible. The windows in the time domain can be set flexibly to cut off these reflected signals. The operator can see the impact of the filter and averaging settings on the dispersion curve instantly.

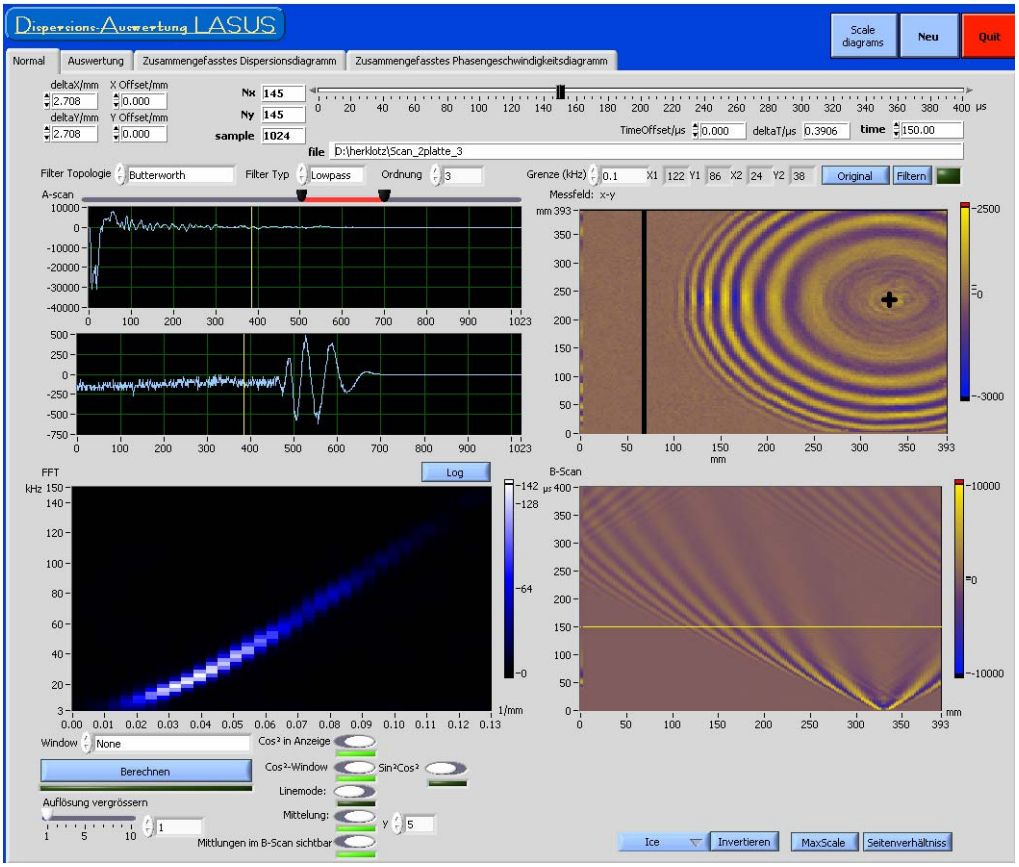

Figure 7. Software surface of the evaluation program. The windows contain: a snapshot of the wave motion (upper right), two time signals at cursor position selected in the snapshots (upper left), a B-scan over the line between the selected cursor positions (lower right) and the dispersion curve (lower left).

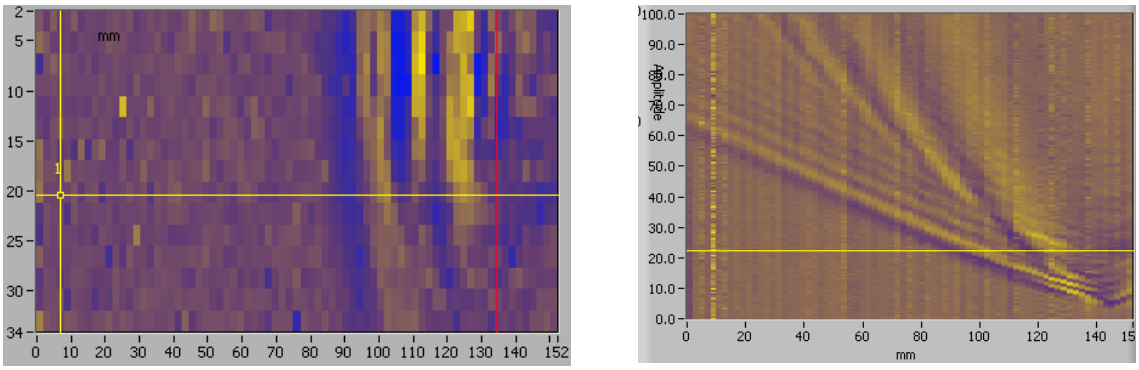

Figure 8. Snapshot (left) and B-scan (right) of the wave field generated by a piezoelectric fiber patch into a Perspex plate of 3 mm thickness.

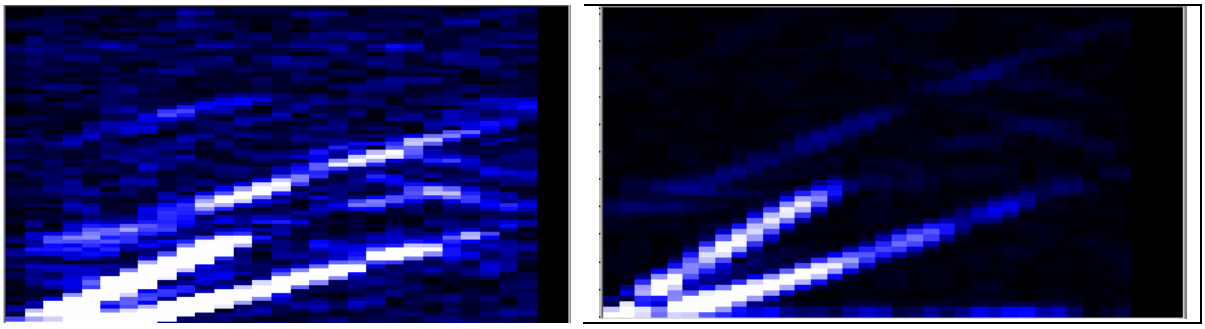

Figure 9. Dispersion maps of the data of Figure 8; left: from row data; right: after cos2 filtering and averaging the measured data over 7 adjacent lines.

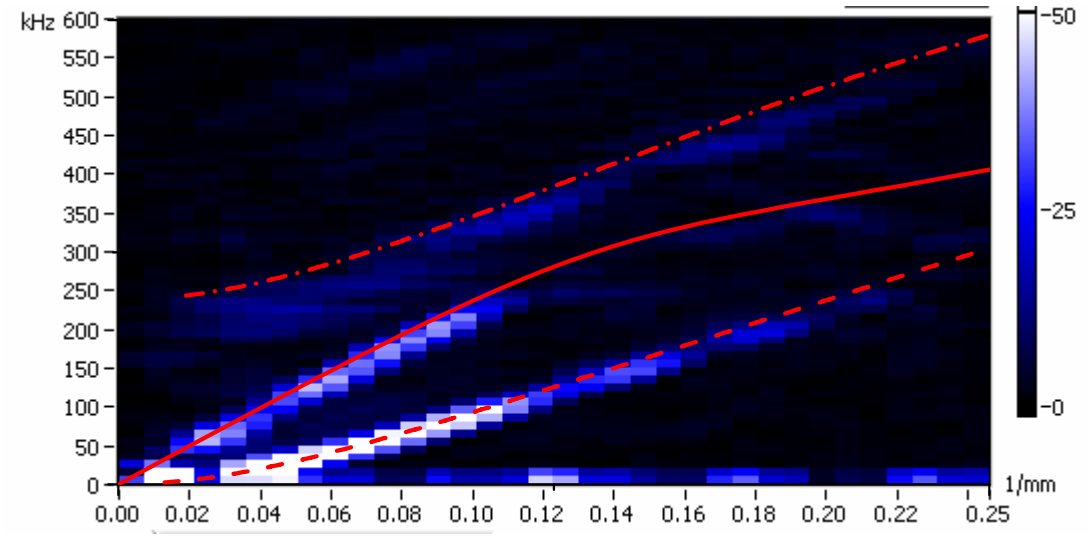

Figure 10. Dispersion map with the calculated dispersion curve swapped; solid line S0, dashed line A0, dashed-dotted line A1; the parameters for the calculation were: c_l = 2.73 mm/µs, c_t = 1.43 mm/µs, d = 3 mm.

Figure 9 shows data from a measurement of the waves traveling in a Perspex plate. The waves are excited by a novel piezoelectric fiber transducer, described in detail in another paper. In this figure the dispersion map obtained using the raw data (left) is compared with the diagram using modified data (right). The modifications consisted in: application of a $\cos^2$ window to cut off noise and possible reflections at the end of the recorded time and

averaging over 7 adjacent lines. It is evident that the signal to noise ratio is improved and some spurious signals disappeared due to the filtering and averaging.

For isotropic material with well known elastic properties the dispersion can be calculated numerically. In Figure 10 the experimentally determined dispersion map is overlaid with the numerically calculated dispersion curve. The three traces in the dispersion map can be clearly identified as A0, S0 and A1 Lamb wave modes.

In the general case the dispersion cannot be calculated due to a lack of precise material parameters. The software developed allows for a semi-automatic (user supported) determination of numerical dispersion curves from dispersion maps, as demonstrated for the measurement of Figure 1. The measurement was driven by a burst with 5 cycles of 500 kHz. This excitation is rather narrow band. Nevertheless, the dispersion map (Figure 11) contains sufficient low frequency data to display the A0 dispersion curve also below 500 kHz. The numerical data for the dispersion curve are compared with the analytical values in Figure 12.

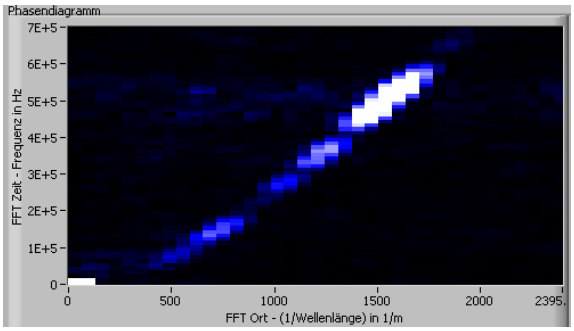

Figure 11. Dispersion map of the measurement of Figure 4.

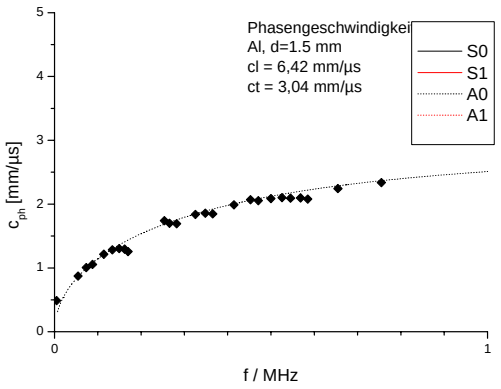

Figure 12. Extracted phase velocity data (points) compared with the numerical results of A0 mode (dashed curve).

6. Application of the Method to Waves in Anisotropic Plates

The GFRP plate with strong anisotropic elastic properties (see chapter 3) is fabricated using a special ply stacking where the 90 degree layer is missing. Snapshots of guided waves are shown in Figure 13. Again two waves can be identified, the fast wave referred to as “S0” and the slow one as “A0”. “S0” reflects the plate anisotropy by the shape of its waveform while surprisingly “A0” has a more or less spherical waveform. In Figure 14 the dispersion map is showing mainly the trace of one mode, most probably “A0”. By choosing appropriate windows in the time domain both modes can be mapped (see Figure 14 bottom). For that, filter parameters are set in such a way that the signals are suppressed for the time after the fast mode having already passed the measurement line.

It was not possible to get orientation dependent dispersion maps which reflect correctly the anisotropy visible in Figure 13. An explanation for this drawback is given by the line length available for generating the dispersion map. If orientations other than the vertical one are considered this length seems to be too small to enable meaningful results. To support this idea a study of the dispersion curves for decreasing evaluation line length has been performed. The vertical orientation with x = 53 mm was used. Starting with the situation displayed in Figure 13 (line length = 85 mm) the lower cursor was set to the y-values 20 mm, 40 mm, 60 mm giving line lengths of 65 mm, 45 mm, and 25 mm, respectively. Figure 15 summarizes the results. The curves for 85 mm and 65 mm are nearly identical. The only difference is that the longer line permits also results for somewhat lower frequen-

cies. But with a decrease of the line length to 45 mm systematic deviations to higher values of phase velocity appear. Finally, the shortest line of only 25 mm yields a totally wrong impression of the dispersion behavior. Now, instead of an increase of the phase velocity with the frequency, the phase velocity is decreasing. While these results are obtained for the slower of both waves ("A0") the situation will be even worse for the faster wave, for which the available line length measured in the number of wavelength is even less.

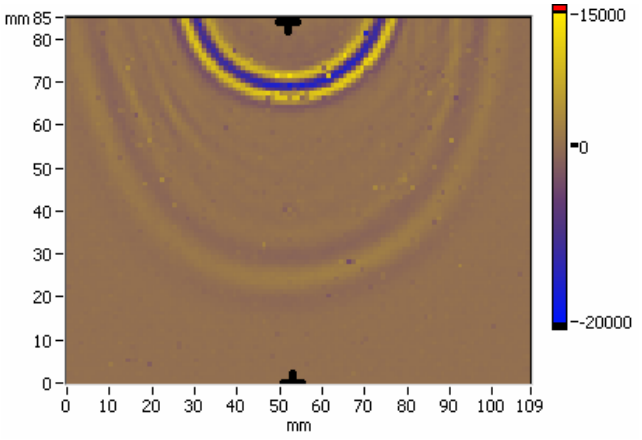

Figure 13. Snapshot of the wave field on a triax GFRP plate. t = 50 µs

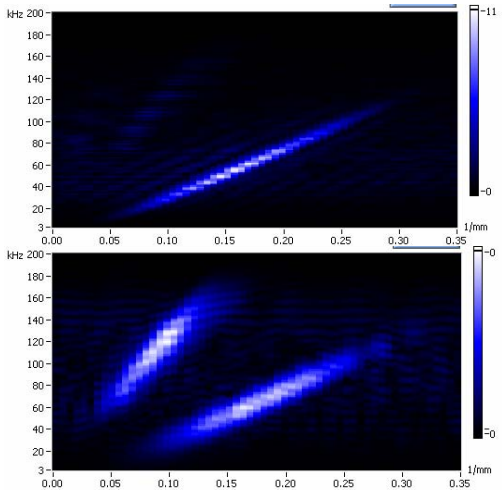

Figure 14. Dispersion map for the vertical line in Figure 13 connecting the two cursor positions. The signals were truncated (cos^2 filter) at t = 400 µs (top) and t = 100 µs (bottom)

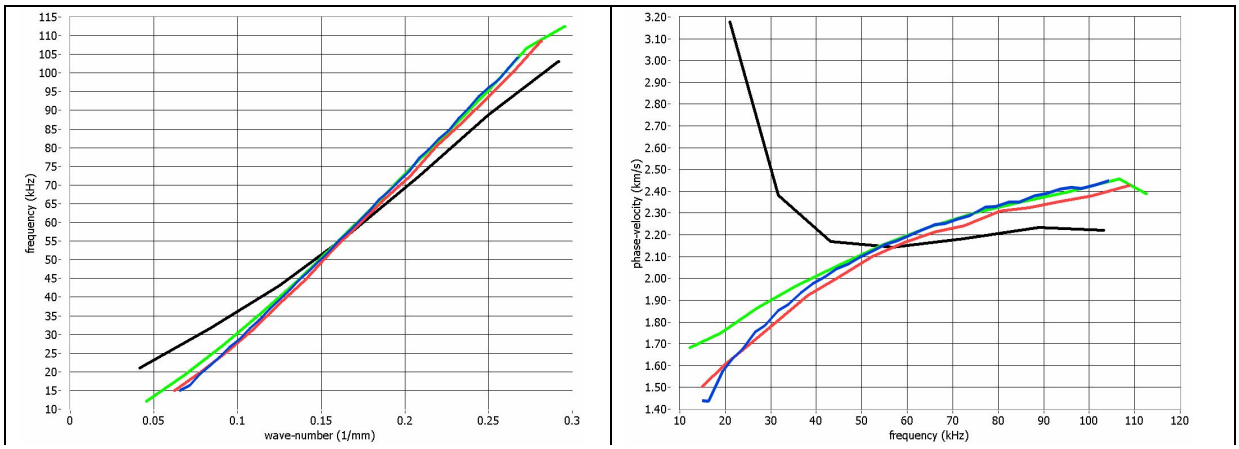

Figure 15. Dispersion diagram of the phase velocity calculated out of the dispersion maps generated with different line length. Left: Frequency versus wave number. Right: Phase velocity versus frequency. The length of the evaluation line amounts for the blue, red, green and black line 85, 65, 45, and 25 mm, respectively.

Summary

Laser vibrometric measurements offer a powerful tool to gather and visualize the wave propagation in plates with isotropic and anisotropic properties. Snapshots and B-scans provide a good qualitative overview of the dispersion. Existing measurements have been used to demonstrate that also quantitative results for dispersion can be attained using a double Fourier transformation technique. While for isotropic plates a good quantitative agreement between experimentally determined dispersion curves and the well known, numerical Lamb wave solutions was demonstrated the case of anisotropic plates needs further work. Here, numerical solutions are not so easy to find. On the experimental side, the data base for evaluating dispersion must be improved. Special measurements will be carried out aiming at acquiring sufficient data to demonstrate the validity of the approach in general, i.e. also in the anisotropic case.

References

[1] B. Köhler, “Recent Progress in Scanning Laser Detection of Pulse-Echo Ultrasound in Concrete”, Journal of Nondestructive Testing, **9** (2004) 1-8

[2] B. Köhler, M. Kehlenbach, R. Bilgram, “Optical Measurement and Visualisation of Transient Ultrasonic Wave Fields”, in: Acoustical Imaging, Vol. **27**, Edited by W. Arnold and S. Hirsekorn, Kluwer Academic/Plenum Publishers, Dordrecht & New York, 2004, 315-322

[3] D. Fei, D.E. Chimenti, “Single-scan elastic property estimation in plates”, Acoustic Research Letters Online, **2** (2001) 49-54

[4] S. D. Holland et al., “Air-coupled, focused ultrasonic dispersion spectrum reconstruction in plates”, J. Acoust. Soc. Am. **115** (6), 2866-2872

[5] B. A. Auld, “Acoustic Fields and Waves in Solids”, Krieger, Malabar, FL, (1990), Vols. 1 and 2

[6] J. D. Achenbach, “Wave Propagation in elastic solids”, Elsevier Science Publishers, B.V. 1990

[7] L. Brekhovskikh, V. Goncharov, “Mechanics of Continua and Wave Dynamics”, Springer Series on Wave Phenomena, Springer Berlin, Heidelberg, New York Tokyo, 1985

[8] D. E. Chimenti, “Guided waves in plates and their use in materials characterization”, Appl. Mech. Rev. **50** (1997) 247–284

[9] S. K. Datta, ‘‘Wave propagation in composite plates and shells,’’ in Comprehensive Composite Materials, edited by T.-W. Chou, Elsevier, Oxford, 2000, Vol. 1

[10] J. L. Rose, “Ultrasonic Waves in Solid Media”, Cambridge University Press, Cambridge, 1999

[11] M. Kehlenbach, B. Köhler, X. Cao, H. Hanselka, “Numerical and Experimental Investigation of Lamb Wave Interaction with Discontinuities”, Proceedings of the 4th International Workshop on Structural Health Monitoring, Stanford University, Stanford, CA, September 15-17, (2003), Proceedings pp. 421-428, ed. by Fu-Kuo Chang, Destech Publications, Inc., 2003